Engineering Structures 344 (2025) 121391

Contents lists available at ScienceDirect

Engineering Structures

journal homepage: www.elsevier.com/locate/engstruct

Full-scale shaking table test, numerical analysis, and design strategy of a prefabricated substation equipment cabin

Jiajun Du [a,b], Wei Wang [a,b,*,1], Jiachen Zhang [a,b], Xiaotian Liu [a,b], Theodoros L. Karavasilis [c]

[a] State Key Laboratory of Disaster Reduction in Civil Engineering & Department of Structural Engineering, Tongji University, Shanghai 200092, China
[b] Shanghai Engineering Research Center for Resilient Cities and Intelligent Disaster Mitigation, Tongji University, Shanghai 200092, China
[c] Department of Civil Engineering, University of Patras, Patras 265000, Greece

ARTICLE INFO

Keywords:
Full-scale shaking table test
Seismic design
Equipment response spectrum
Prefabricated substation equipment cabin

ABSTRACT

This paper presents both experimental and numerical investigations of a prefabricated cabin, which serves as a core component of the new generation of intelligent, modular substations. A bidirectional full-scale shaking table test was conducted to examine the dynamic characteristics and seismic responses of the prefabricated cabin structure and the equipment mounted within it. The test results demonstrate that the prefabricated cabin satisfies the structural requirements of a seismic design intensity of 8 according to Chinese code. Subsequently, a corresponding finite element model was developed and validated using the experimental data. Based on this validated model and inspired by the concept of floor response spectra, numerical analyses were conducted to explore the peak acceleration response and acceleration amplification factors of switchgear and panel-type equipment placed in the cabin across a range of natural periods. These results provide practical insights into mitigating equipment seismic responses. Furthermore, to support structural design, a dimensionless parameter — the response spectrum stiffness ratio (η) — is proposed. It is defined as the ratio between the actual lateral structural stiffness to the stiffness demand derived from the design acceleration spectrum corresponding to the rare-level earthquake. Then, a series of parametric analyses were performed with the validated finite element model to identify applicable ranges of η under different seismic design intensities, ultimately leading to a recommended design strategy for prefabricated cabins.

1. Introduction

In modern society, reliable power infrastructure is of critical importance, serving as the backbone for essential services ranging from healthcare and communication to industrial production and residential needs. As nodal hubs in power systems, substations play a pivotal role in voltage transformation, electricity distribution, and system protection, making their operational integrity fundamental to grid stability [1]. Consequently, seismic vulnerability studies of substations have emerged as a pivotal aspect in enhancing infrastructure resilience. Historical seismic events, such as the 2008 Wenchuan earthquake in China, demonstrate that prolonged outages resulting from substation failures can lead to significant economic losses and recovery challenges [2]. This underscores the imperative for the prioritization of resilient substation designs in high-risk zones, with the objective of safeguarding grid functionality and averting catastrophic societal impacts during seismic events.

In light of this, many researchers have conducted extensive study into the seismic performance of substations. Zhu et al. [3] proposed refined seismic fragility curves of a 500 kV power transformer considering ground motion classifications. Considering interconnected systems and independent configurations of substations, Taghizadeh et al. [4] explored the optimal method for seismic intensity measurements of high-voltage substation equipment. Beyond theoretical modeling, practical mitigation strategies have also gained attention. For instance, Li et al. [5] demonstrated the efficacy of double friction pendulum-based isolation in enhancing the seismic performance of transformer-bushing systems, while He et al. [6] employed wire rope isolators to reduce the seismic life cycle cost of ultra-high voltage bypass switches. Furthermore, with the consideration of seismic failure correlation between equipments, Liang and Xie [7] conducted probabilistic seismic risk analysis of a substation. Meanwhile, Liu and Xie [8] proposed a multi-stage seismic resilience improvement evaluation framework for substations. These valuable studies have deepened the knowledge of the seismic performance of substation systems, but are mainly limited to the conventional substation rather than the new prefabricated cabin-type substation.

* Correspondence to: State Key Laboratory of Disaster Reduction in Civil Engineering, Tongji University, Shanghai, 200092, China.
E-mail address: weiwang@tongji.edu.cn (W. Wang).
[1] Professor.

https://doi.org/10.1016/j.engstruct.2025.121391
Received 16 April 2025; Received in revised form 8 August 2025; Accepted 13 September 2025
Available online 22 September 2025

(a) Conventional substation. (Adapted from [9]) (b) Prefabricated cabin-type substation.(Adapted from [10])

Fig. 1. Photos of different substation types (see [9,10]).

Prefabricated cabin-type substations are fundamentally different from conventional substations in terms of their configuration and other aspects (as shown in Fig. 1). Generally, they adopt a modular integrated design, choosing a standardized steel cabin to highly integrate primary equipment (transformer, switchgear), secondary protection system, environmental monitoring, and so on, forming a "plug-and-play" power unit, breaking the limitations of the conventional decentralized substation design. This new type of substation has many advantages, including a short construction period, flexible deployment, low carbon emissions during production, and high environmental adaptability (cold weather, etc.), and has therefore gained a lot of traction in recent years with governments and companies.

However, the current research on prefabricated cabin-type substations is scarce, mainly focusing on the discussion of its construction and technical advantages [11,12], with few studies on the seismic performance of the prefabricated substation equipment cabin (PSEC). Some studies have explored the mechanical behavior of PSECs under specific working conditions through static analysis using finite element software [13,14]. While other studies can serve as references for shaking table tests of PSECs. For example, Congru et al. [15] performed shaking table tests on a scaled concrete indoor substation model with lead rubber bearings and viscous dampers, while Chen et al. [16] investigated a scaled steel indoor substation model with a partial isolation system, both aiming to evaluate seismic performance under near-fault and far-field ground motions. However, these indoor substation concrete or steel frames are not the same as the prefabricated cabin structures studied in this paper. Feng et al. [17] proposed a resilient steel frame with replaceable buckling-restrained cover plates for energy dissipation and disc spring bolts for restoring force, replacing conventional frames under prefabricated cabins. These studies have provided valuable insights into the static analysis and seismic mitigation measures for prefabricated cabins, but as with other structures in preparation for expanded application in high seismic intensity zones, more shaking table test validation, dynamic time history analysis, etc., for prefabricated cabin structures are still necessary until reliable design recommendations or specifications can be developed. Additionally, compared to other structures, the differences in the dynamic characteristics of prefabricated cabin structures due to their size, mass, and the spacing of the beams and columns to serve functions (e.g., equipment placement, cable passages, and maintenance) emphasize the need for shaking table tests to provide a reliable technical basis for further finite element analysis, design methods, and so on.

Based on the above, this paper presents a bidirectional full-scale shaking table test and numerical analysis of a practical two-story prefabricated substation equipment cabin, and proposes a corresponding structural design strategy. The rest of the paper is organized as follows: Section 2 presents the full-scale shaking table test program, including the tested prefabricated cabin, instrumentation, and loading protocols. This is followed by discussions of the shaking table test results in Section 3. Subsequently, numerical analysis based on the experimentally validated finite element model is conducted, with Section 4 investigating the response spectra of the equipment in the tested prefabricated cabin and Section 5 giving a feasible structural design strategy. Finally, main findings and some limitations in this study are presented in Section 6.

2. Shaking table test of the actual engineering-use PSEC

2.1. Test model

The test model used in this study is a full-scale prototype of a two-story prefabricated steel cabin for substation equipment, which was designed and constructed based on an actual engineering project. It is designed for a seismic intensity of 8 (peak ground acceleration (PGA) corresponding to a 475-year return period, PGA_{475y}, is 0.3 g). The site characteristic period is 0.65 s. As shown in Fig. 2, the cabin consists of two vertically stacked steel modules with story heights of 3.62 m and 2.95 m for the first and second floors, respectively. The entire structure is anchored to the shaking table via four fixed supports. Each floor comprises two symmetrically arranged modules, which are connected both horizontally and vertically using friction-type high-strength bolts. The cross-sectional dimensions of the structural members are provided in Table 1. The model elevation includes a door lintel (a transverse short beam used to install and secure wall panels), which is formed into a C-shaped cross-section from 2.5 mm thick steel plates by cold bending, with a cross-sectional height of 100 mm and a width of 70 mm. Additionally, lateral bracing steel plates are provided: in the short (X) direction, they are 320 mm wide, and in the long (Y) direction, 440 mm wide. All steel plates are 5 mm thick, and each bracing plate is stiffened with four square hollow sections of 40 × 40 × 3 mm. The steel used for all structural components in the test model is Q355, with a yield strength f_y = 355 MPa. The mass of the first story of the test model is approximately 9.8 tons, including two symmetrically installed switchgear cabinets, each weighing about

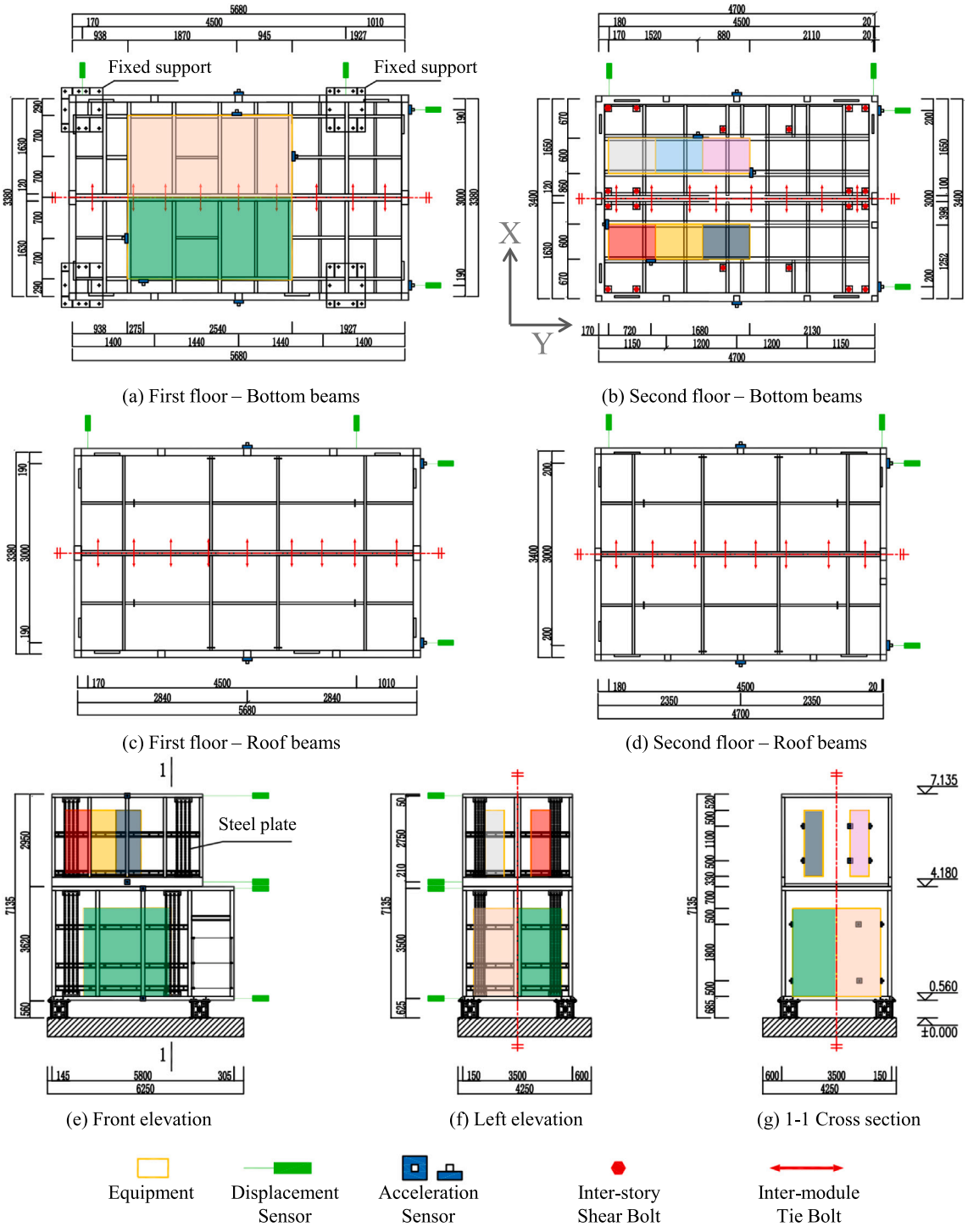

Fig. 2. The illustration of test model.

2.8 tons. The second story has a total mass of about 4.5 tons, with six symmetrically arranged panel cabinets, each weighing approximately 0.2 tons. The equipment on the first floor is bolted to angle steel welded to the side of the bottom beam, while the equipment on the second floor is bolted to equipment brackets welded to the bottom beam of the floor, as shown in Fig. 3. The fixed supports contribute an additional mass of around 1.6 tons, bringing the total mass of the model to approximately 16 tons. Fig. 4 shows the photo of the test model. Notably, the test model was designed without maintenance steel plate walls to facilitate observation of the structural components and internal equipment during the shaking table test. Additionally, the absence of these walls mitigated safety risks associated with potential detachment and falling into the shake table.

Notably, the spatial arrangement of the beam and column elements, as well as the quantity and layout of the equipments in the test model, were all derived from the specific requirements of the engineering project. In particular, the former was primarily designed to support equipment loads, accommodate cable routing, and ensure accessibility for maintenance. While the sizes of the structural components are

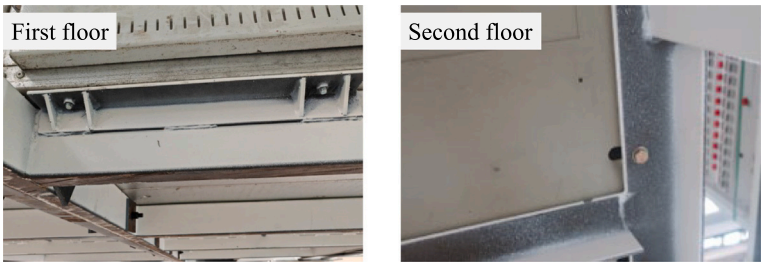

Fig. 3. The illustration of equipment anchoring methods.

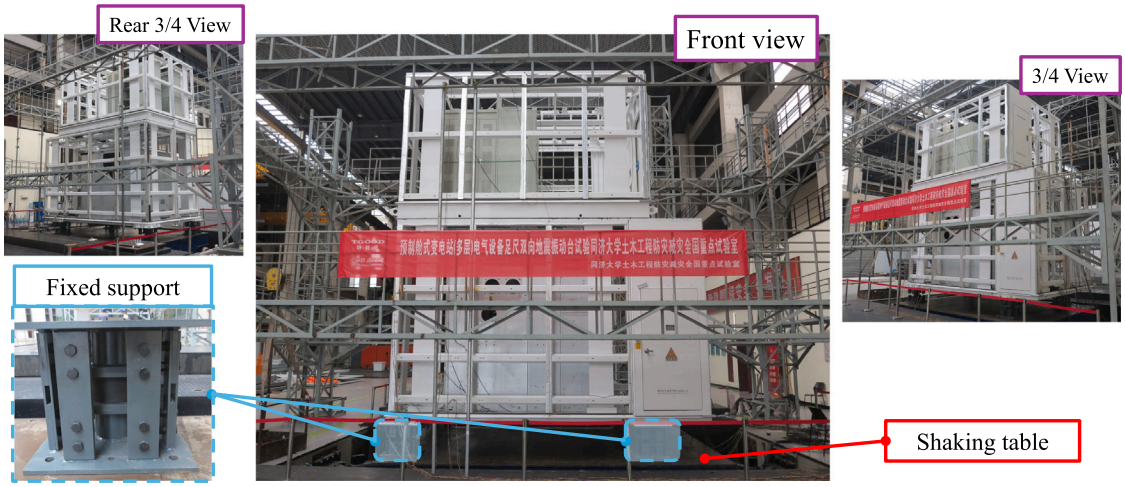

Fig. 4. The photo of the test model.

Table 1
Cross-section of the test model.

Name	Cross-sectional specification
Column of the 1st-floor module	□120 × 120 × 6
Column of the 2nd-floor module	□100 × 100 × 4
Lower beam beneath 1st-floor column	□120 × 120 × 8
Main beam on 1st floor	□120 × 60 × 4
Secondary beam on 1st floor	□40 × 40 × 3
Upper beam of the 1st-floor column	□120 × 120 × 6
Other top beams on 1st floor	□80 × 40 × 5
Lower beam beneath 2nd-floor column	□300 × 150 × 6
Transverse beam in Y-direction (2nd floor)	H100 × 100 × 6 × 8
Secondary beam on 2nd floor	□100 × 50 × 3
Upper beam of the 2nd-floor column	□100 × 100 × 4
Other top beams on 2nd floor	□80 × 40 × 5

selected according to the requirements of the Chinese code (GB/T 50017-2017) [18].

2.2. Test setup and instrumentation

The shaking table test was conducted in the multifunctional shaking table laboratory of the Earthquake Engineering Hall at Tongji University (Jiading Campus). The shaking table used has dimensions of 6.0 m × 4.0 m, with a maximum effective load capacity of 30 tons. Its rated acceleration and displacement amplitude are ±1.5 g and ±500 mm, respectively, and the operating frequency range is from 0.1 to 50 Hz. To measure the absolute acceleration of the structure, one acceleration sensor was installed in each of the X and Y directions at the centroidal height of the top and bottom beams on both the first and second floors. Additionally, dynamic displacement sensors (Linear Variable Differential Transformers, LVDTs) were installed at the same height as the acceleration sensors, with two sensors in each direction, to measure both translational and torsional floor displacements. To capture the equipment response, two acceleration sensors were mounted along the height of the equipment at two corner locations on each floor. The lower sensor was placed at a distance from the base, as pre-test analysis indicated that the connection at the equipment's base would remain safe, allowing the floor acceleration to serve as a proxy for the equipment's base input. The upper sensor was then arranged symmetrically. Notably, this study focuses on the equipment acceleration response rather than displacement, as a review of existing literature [19,20] indicates that damage to substation equipment and its internal components is predominantly governed by acceleration. While component-level seismic performance is often evaluated through displacement limits in single-cabinet tests [20], our research investigates a complete, integrated "structure-equipment" system. This approach yields equipment acceleration amplification factors (see Section 4), which are critical for establishing a holistic performance criterion. Specifically, these factors allow the well-established displacement limits of individual equipment to be translated into an equivalent acceleration limit at the base of the entire system [20]. Fig. 2 illustrates the detailed arrangement of the acceleration and displacement sensors for the shaking table tests.

2.3. Input seismic ground motions and test cases

Bidirectional ground excitations were applied to the test model. According to Chinese code GB 50011-2010 [21], three ground motion records were selected and scaled, including one artificial ground motion, one near-fault ground motion, and one far-field ground motion. Their response spectra, along with the design spectrum, are shown in Fig. 5. Besides, the detailed information (e.g., magnitude and duration) and time histories are presented in Table 2 and Fig. 6.

The experiment was conducted with five stages of horizontal bidirectional seismic loading combinations at PGAs of 0.1 g, 0.2 g, 0.3

Table 2
Summary of ground motion information.

Ground motion	Type	Year	Magnitude	Station	PGA (/g)	PGV (cm/s)	Time step (s)	Duration (s)
SAEWs	Artificial	–	–	–	0.30	46.5	0.01	20.00
Landers	Far-field	1992	7.3	Yermo fire	0.24	52.0	0.02	44.00
Cape Mendocino	Near-fault	1992	7.0	Petrolia	0.63	82.1	0.02	36.00

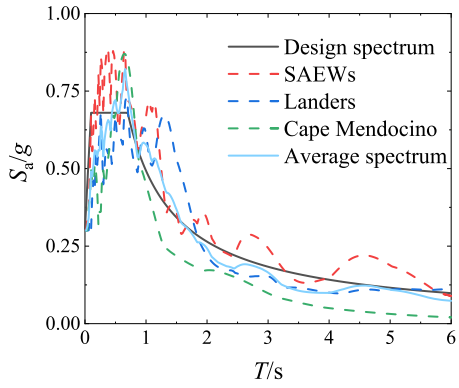

Fig. 5. Acceleration spectra of selected ground motions scaled to 0.3 g.

g, 0.51 g, and 1.00 g (X: Y = 0.85:1 or 1:0.85), corresponding respectively to frequent earthquakes with relatively small amplitudes and higher probabilities of occurrence (0.1 g, 0.2 g), the basic-level design earthquake (0.3 g, return period of 475 years), the rare-level earthquake (0.51 g, return period of 2475 years, as specified in the Chinese code [21] for seismic design intensity 8, PGA_{475y} = 0.3 g), and a highly destructive seismic scenario (1.00 g). After completing each loading stage, except for the initial condition, a white noise frequency sweep (X: Y = 1:1) was performed to detect changes in the structural dynamic characteristics. The loading conditions are shown in Table 3.

3. Shaking table test results

3.1. Dynamic characteristic

The basic dynamic parameters of the test model primarily refer to the structure's natural period and damping ratio, which were calculated based on the white noise case in the experiment. To obtain these parameters, the absolute acceleration time history of the shaking table surface was used as the input, and the absolute acceleration time history at the top of the second floor was recorded as the output. By applying the transfer function between the input and output, an amplitude–frequency diagram is derived. The structure's natural frequency can be identified from the peak value of this diagram, from which the natural period is then calculated. The damping ratio of the structure can also be obtained from the amplitude–frequency diagram by using the half-power bandwidth method. Table 4 shows the results for the calculated natural period and damping ratio. It can be observed that the first periods in the X and Y directions of the prefabricated substation cabin both fall within the platform section (0.1 s to 0.7 s) of the design response spectrum. The structural damping ratio is higher than that of typical steel structures, which is attributed to factors such as ongoing equipment vibrations, friction, and impacts from auxiliary components during the experiment. This result aligns with relevant standards and research findings, where damping ratios for electrical equipment, such as equipment cabinets, can range from 3.7% to 13.9% [20,22,23].

3.2. Acceleration responses

3.2.1. Acceleration of the structure

Fig. 7 illustrates the peak absolute acceleration responses at representative measurement points on the structure under various loading cases. It can be observed that, for the prefabricated cabin, the two measurement points located on different floors but in the same horizontal direction exhibit similar trends in peak acceleration responses, generally increasing with height. Due to the higher spectral acceleration at short periods and the denser waveform characteristics of the artificial ground motions, which imply higher input energy, the largest peak acceleration responses are typically observed under artificial wave conditions. This phenomenon is particularly pronounced at the top of the second floor in the X direction. At the five loading levels with PGAs of 0.1 g, 0.2 g, 0.3 g, 0.51 g, and 1.00 g, the average peak accelerations at the top of the first floor are approximately 0.17 g, 0.37 g, 0.53 g, 0.76 g, and 1.72 g, respectively; while those at the top of the second floor are approximately 0.25 g, 0.57 g, 0.79 g, 1.1 g, and 2.21 g, respectively. Overall, the acceleration amplification factors relative to the input ground motions range approximately from 1.0 to 2.5.

Table 3
Test cases.

Loading Condition	PGA /g	Input Excitation	Amplitude-Expected(Actual)/g		Duration /s
			X Direction	Y Direction	
1	0.1	White noise	0.050 (0.042)	0.050 (0.050)	100.0
2		SAEWs	0.100 (0.105)	0.085 (0.088)	20.0
3		Landers	0.100 (0.091)	0.085 (0.079)	44.0
4		Cape Mendocino	0.100 (0.097)	0.085 (0.087)	36.0
5		SAEWs	0.085 (0.089)	0.100 (0.102)	20.0
6		Landers	0.085 (0.080)	0.100 (0.089)	44.0
7		Cape Mendocino	0.085 (0.085)	0.100 (0.102)	36.0
8		White Noise	0.050 (0.043)	0.050 (0.051)	100.0
9	0.2	SAEWs	0.200 (0.208)	0.170 (0.183)	20.0
10		Landers	0.200 (0.237)	0.170 (0.194)	44.0
11		Cape Mendocino	0.200 (0.195)	0.170 (0.177)	36.0
12		SAEWs	0.170 (0.177)	0.200 (0.212)	20.0
13		Landers	0.170 (0.201)	0.200 (0.233)	44.0
14		Cape Mendocino	0.170 (0.173)	0.200 (0.205)	36.0
15		White Noise	0.050 (0.043)	0.050 (0.051)	100.0
16	0.3	SAEWs	0.300 (0.326)	0.255 (0.284)	20.0
17		Landers	0.300 (0.356)	0.255 (0.302)	44.0
18		Cape Mendocino	0.300 (0.294)	0.255 (0.264)	36.0
19		SAEWs	0.255 (0.281)	0.300 (0.328)	20.0
20		Landers	0.255 (0.309)	0.300 (0.348)	44.0
21		Cape Mendocino	0.255 (0.261)	0.300 (0.307)	36.0
22		White Noise	0.050 (0.043)	0.050 (0.050)	100.0
23	0.51	SAEWs	0.510 (0.491)	0.434 (0.426)	20.0
24		Landers	0.510 (0.573)	0.434 (0.499)	44.0
25		Cape Mendocino	0.510 (0.491)	0.434 (0.435)	36.0
26		SAEWs	0.434 (0.426)	0.510 (0.524)	20.0
27		Landers	0.434 (0.485)	0.510 (0.573)	44.0
28		Cape Mendocino	0.434 (0.393)	0.510 (0.491)	36.0
29		White Noise	0.050 (0.043)	0.050 (0.050)	100.0
30	1.00	Cape Mendocino	1.000 (1.165)	0.850 (1.018)	36.0
31		Landers	1.000 (1.274)	0.850 (1.082)	44.0
32		SAEWs	1.000 (0.929)	0.850 (0.790)	20.0
33		White Noise	0.050 (0.041)	0.050 (0.049)	100.0

Table 4
Structural natural period and damping ratio.

	X direction	Y direction
Period/s	0.202	0.165
Damping ratio/%	8.7	6.8

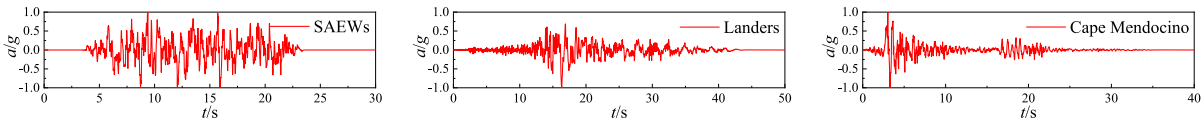

(a) Record of SAEWs. (b) Record of Landers. (c) Record of Cape Mendocino.

Fig. 6. Acceleration history of ground motions.

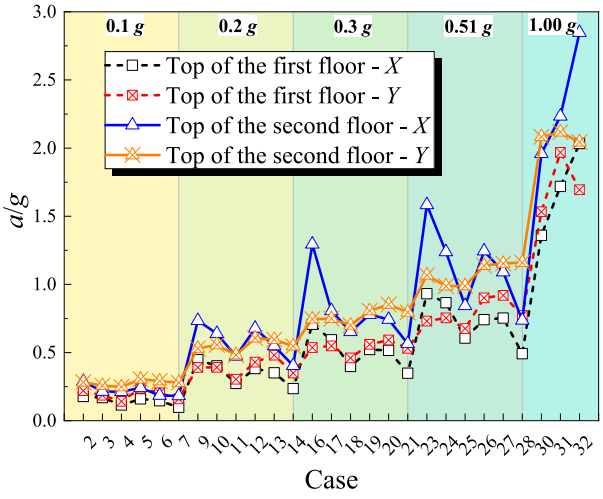

Fig. 7. Peak absolute acceleration response of the structure.

3.2.2. Acceleration of equipment

During the tests, no significant damage to the equipment was observed under all loading cases with PGA ≤0.51 g. When the PGA reached 1.0 g, the equipment on the first floor still showed no evident damage, while the equipment on the second floor exhibited several forms of physical failure, including shearing of the bottom connection bolts, tearing of the base plate, detachment from the support frame, and a noticeable overall tilt, as shown in Fig. 8.

Fig. 9 presents a comparison of the absolute acceleration time histories between the measurement point at the top of the second-floor structure and that at the upper part of the equipment on the same floor. It can be observed that, compared to the structure, the equipment generally exhibits dynamic characteristics of higher amplitude and frequency. This phenomenon occurs due to the relatively low stiffness of the frames and panels of the equipment on which the accelerometers are mounted, resulting in a relatively high local dynamic response at the measurement point.

Fig. 10 illustrates the peak acceleration responses of the equipment on the first and second floors under different test cases. In most cases with a Peak Ground Acceleration (PGA) less than 0.51 g, such as in Case 10 (0.2 g PGA), the peak response of the second-floor equipment slightly exceeded that of the first floor. However, at higher PGA levels of 0.51 g and 1.0 g, this trend reverses, with the first-floor equipment exhibiting a significantly, and somewhat anomalously, higher peak acceleration than the second-floor equipment. To investigate this behavior, the floor acceleration response spectra were firstly analyzed. As shown in Fig. 11, the spectral response of the second-floor equipment is consistently higher than that of the first floor across the two different PGA levels, which contradicts the peak acceleration observations at higher intensities. This discrepancy is attributed to the difference in sensor installation locations. The first-floor accelerometer was mounted on an external panel of the cabinet, whereas the second-floor sensor was mounted to a cabinet frame column. This explanation is further substantiated by the Fourier spectrum analysis of the floor and equipment responses, presented in Fig. 12. The spectra indicate that the signal from the first-floor accelerometer contains significant high-frequency components, which become particularly pronounced at the 0.51 g PGA level. These components are indicative of localized panel vibrations, driven by the panel's lower out-of-plane stiffness. In contrast, the signal from the second-floor sensor on the cabinet frame column shows less such high-frequency contamination. This finding underscores that for accurate assessment, accelerometers should be mounted on equipment rigid elements, as measurements from flexible panels can yield misleading data regarding the damaging response experienced by the equipment.

3.3. Displacement responses

Fig. 13 presents the peak relative displacement responses at representative structural measurement points under different cases. It can be observed that the peak relative displacements of the two floors follow a similar trend. As shown in Fig. 14, the maximum relative displacement between the top of the first floor and the bottom of the second floor is approximately 4 mm under 1.0 g PGA. Considering potential measurement errors, this indicates that no significant inter-story slip occurred, suggesting that the high-strength bolts connecting the floors maintained reliable performance throughout the tests. Under conditions with PGA less than 0.51 g, the maximum inter-story drift ratio of the prefabricated cabin model was 1/319, which is well within the code-specified limit (1/50) for rare-level earthquakes [21]. No significant plastic deformation, damage, or residual displacement was observed in the steel cabin during the tests, further confirming that the cabin did not experience excessive inter-story deformation under the specified seismic conditions.

4. Equipment acceleration response spectrum

In recent years, the seismic performance and design methodologies of non-structural components have attracted significant research attention [24]. Among these efforts, the floor response spectrum (FRS) has emerged as a valuable tool for the seismic design of non-structural components. FRS is typically obtained by inputting the absolute acceleration time histories at a floor into dynamic models of non-structural components with varying natural periods. Inspired by the concept of FRS, this study investigates the peak equipment acceleration (PEA) with different natural periods placed within the tested prefabricated cabin model, under rare-level earthquakes corresponding to design seismic intensity 8. These acceleration profiles are hereafter referred to as the "equipment response spectrum" (ERS).

The ERS is obtained through extensive numerical analyses based on the finite element model developed by SAP2000. A two-stage approach is adopted for the numerical modeling of the structure-equipment system. Initially, the Finite Element (FE) model of the primary structure is developed and validated against experimental data to ensure an accurate representation of its dynamic characteristics; at this stage, the equipment is represented solely by its mass applied to the floors via shell elements, as presented in Fig. 15. The equipment mass is adjusted by modifying the thickness of the elements. Additionally, the beams and columns of the prefabricated cabin are modeled using 'frame' elements, while the lateral bracing steel plates are modeled by 'thin-shell' elements. All components in the test model are fabricated from Q355 steel, with the yield strength set to 355 MPa. All beam–column connections

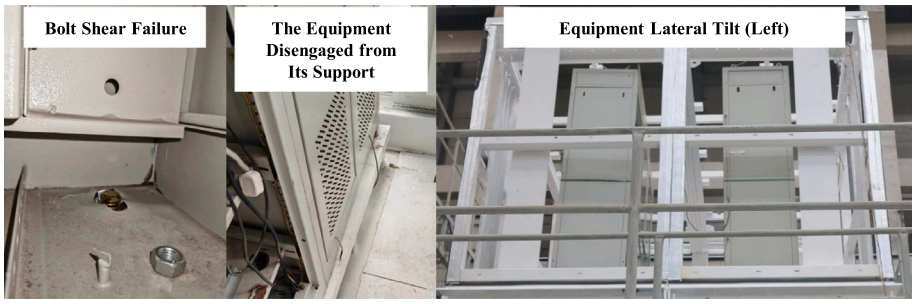

Fig. 8. Equipment damage.

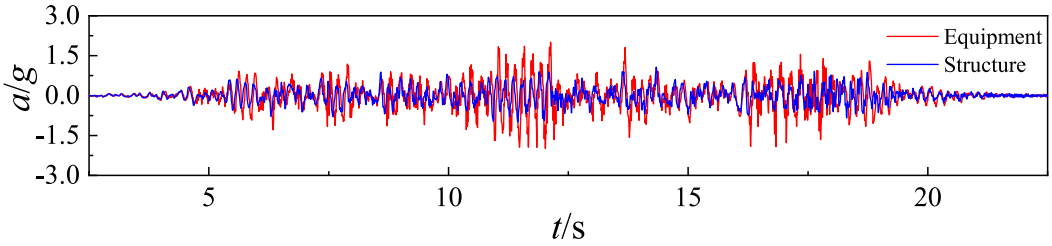

Fig. 9. Comparison of absolute acceleration time histories between the top-floor measurement point of the structure and the upper equipment measurement point on the second floor in the Y direction.

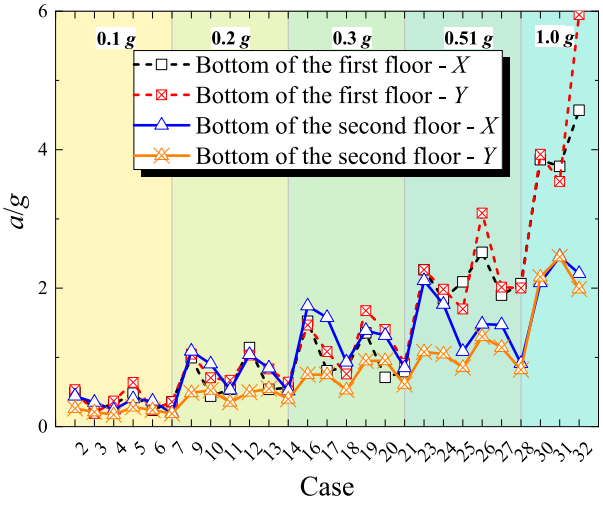

Fig. 10. Peak absolute acceleration responses of the equipments.

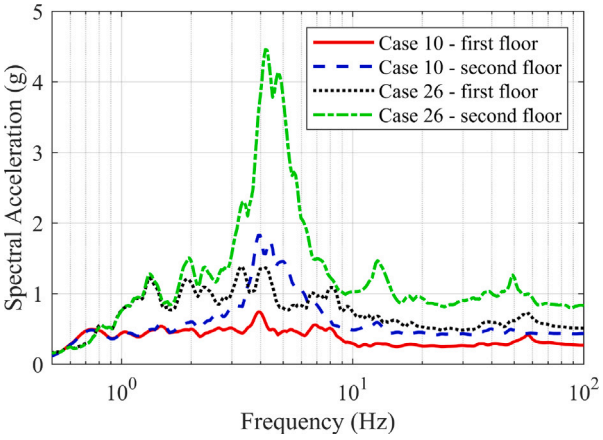

Fig. 11. Floor response acceleration spectrum (Case 10 and 26).

are defined as rigid. As each connection point between the equipment and the base beams or brackets utilizes a single friction-type high-strength bolt, these connections are modeled as hinged by constraining their three translational degrees of freedom. The fundamental periods of the finite element model in the X and Y directions were 0.211 s and 0.152 s, respectively, which show a good match with the experimental periods of 0.202 s and 0.165 s. Fig. 16 presents a comparison between the typical acceleration and displacement time histories from the finite element simulation and the experimental results. The good agreement between the results demonstrates the reliability and accuracy of the finite element model. Notably, several factors could account for the discrepancies between the numerical and experimental results. These potential sources include: the difference between the actual material strength of the test model and its nominal strength; local or global imperfections introduced by fabrication errors in the structural system; and errors in equipment installation or deviations between the equipment's actual and nominal mass. Furthermore, the discrepancies may also be attributed to factors not considered in the finite element model, such as the local vibration of the equipment cabinet and its internal components, as well as their unique damping characteristics.

Subsequently, a simplified equipment model, composed of two shell elements and four rectangular columns representing its primary frame, is integrated into the validated structural model, as shown in Fig. 17. The height of the simplified model matches that of the actual equipment (2.8 m for the first-floor equipment and 2.1 m for the second-floor equipment). The equipment mass is applied to the top and bottom surface elements and equally distributed in a 1:1 ratio, with each surface carrying half of the actual mass. Variations in the equipment's natural period were achieved by adjusting the cross-sectional dimensions of the four columns. This modeling strategy is justified as it conceptually extends the FRS method by analyzing the equipment's overall response to floor motions. Furthermore, it captures the essential physical behavior wherein the cabinet's lateral stiffness is predominantly provided by its frame. While this simplified model does not resolve localized phenomena like panel vibrations, it represents a deliberate trade-off between analytical detail and computational feasibility. A high-fidelity, fully coupled model capable of simulating such local effects would be computationally prohibitive and require separate, extensive experimental calibration. The adopted approach, therefore, aims to efficiently

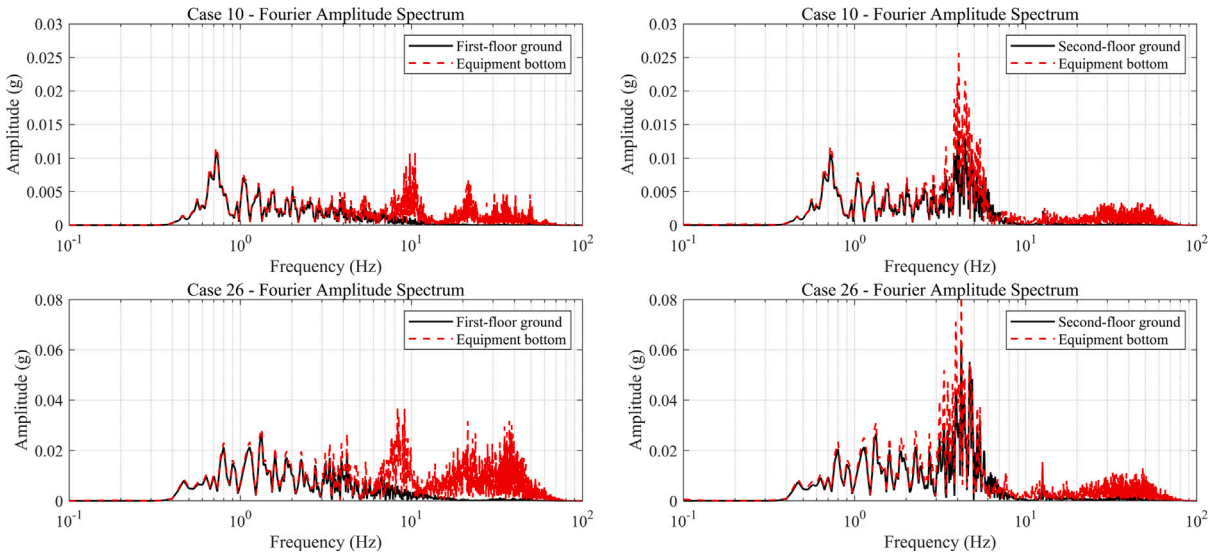

Fig. 12. Fourier spectrum of the acceleration responses (Case 10 and 26).

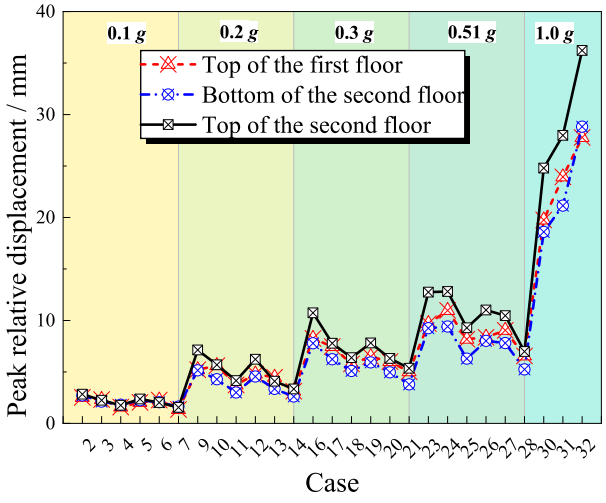

Fig. 13. Peak relative displacement response of the structure.

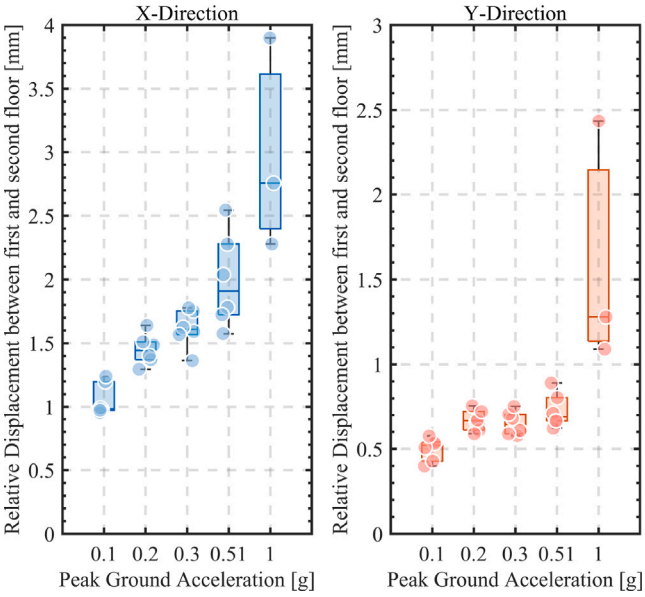

Fig. 14. Maximum relative displacement between first and second floor.

generate robust equipment response spectra suitable for engineering design purposes.

The PEA with varying natural periods are then obtained through time history analyses. Existing research [19,20,22,25–27] and manufacturer experience indicate that the investigated equipment cabinets in prefabricated substations are generally quite stiff, possessing short natural periods. For instance, the natural period was approximately 0.05 s for both the switching power cabinet studied by Zuo et al. [19] and the metal-clad switchgear investigated by Iijima et al. [27]. While longer periods have been reported, such as the power distribution cabinets studied by Shang et al. [20] with a maximum period approaching 0.3 s, even longer periods seem uncommon. This observation is corroborated by the experience of the substation cabins' manufacturer. Accordingly, a period range of 0.05 s to 0.5 s (with an interval of 0.025 s for the time history analyses) was adopted in this study to align with findings from the literature and prevailing practices. The input ground motions consisted of 50 earthquake records recommended by FEMA P695 [28], including 22 far-field and 28 near-field records. As detailed in the P-695 report, these records were selected with the objective of creating a standardized, general-purpose suite of ground motions. This suite is intended to be representative of a broad range of common site

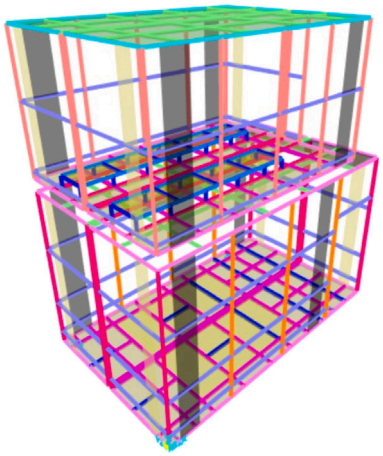

Fig. 15. Validated finite element model.

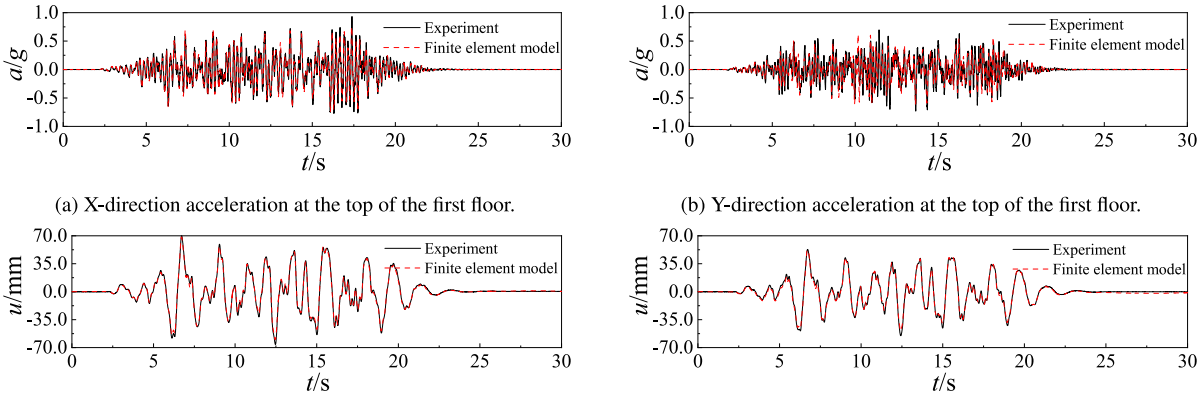

(a) X-direction acceleration at the top of the first floor.

(b) Y-direction acceleration at the top of the first floor.

(c) X-direction displacement at the top of the first floor.

(d) Y-direction displacement at the top of the first floor.

Fig. 16. Comparison of finite element simulation and experimental time history under case 23.

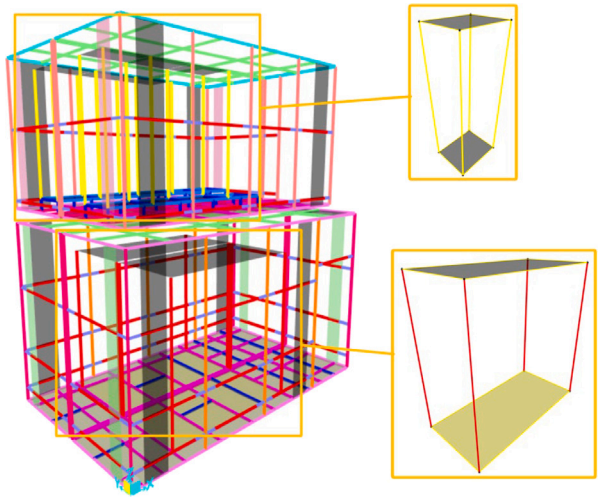

Fig. 17. Finite element model for ERS analysis. (For interpretation of the references to color in this figure legend, the reader is referred to the web version of this article.)

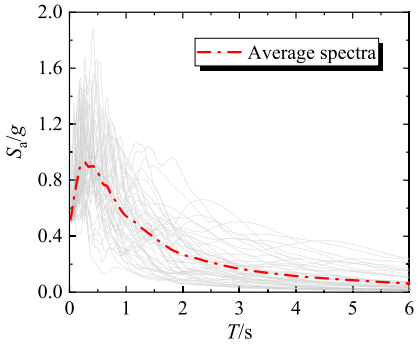

Fig. 18. Acceleration response spectra of 50 scaled ground motions.

conditions and sufficiently destructive to be suitable for evaluating and comparing various types of structural systems. The selection process was governed by rigorous criteria, including the number of earthquake events, magnitude, epicentral distance, site conditions, fault type, and PGA, etc., all of which are thoroughly elaborated in the FEMA P-695 report. Considering that the ERS study conducted here aims to provide results with a certain degree of generality, it is reasonable to use this set of ground motions. For practical applications where the interest is confined to a specific site, a more targeted ground motion selection based on local site conditions could certainly be performed to obtain site-specific ERS results. The amplitude-scaled acceleration response spectra of these ground motions are shown in Fig. 18, with the damping ratio set to the experimentally measured value of 8.7%.

The aforementioned ground motions (PGA = 0.51 g, X:Y = 1:0.85) are applied to the model, and the PEA curves for the first- and second-floor equipment are shown in Fig. 19. It can be observed that the average ERS curves of the first-floor equipment in the X, Y, and bidirectional square root of the sum of the squares (SRSS)-combined directions exhibit a certain degree of fluctuation, with values ranging from 1.50 g to 2.03 g (X), 1.50 g to 1.78 g (Y), and 2.18 g to 2.51 g (SRSS), respectively, but without any significant increasing or decreasing trend within the period range. In contrast, the ERS curves for the second-floor equipment exhibit distinct single-peak characteristics: the X-direction curve reaches a maximum of 5.00 g at 0.2 s, the Y-direction curve peaks at 3.68 g at 0.15 s, and the bidirectional SRSS-combined curve reaches a maximum of 5.64 g at 0.2 s.

For practical engineering application, the design response spectra were fitted using the upper bounds of the 95% confidence intervals of the data points on each curve. Based on the characteristics of the ERS curves for equipment on the first and second floors, the design response spectrum for the first-floor equipment adopts the median value (2.697 g) of the upper bounds within the period range, while that for the second-floor equipment is fitted as a piecewise linear function using the least squares method. Fig. 20 presents the recommended bidirectional SRSS-combined design response spectra for equipment, and the functional expression for the second-floor equipment is given in Eq. (1). The fitted function for the second-floor equipment achieves an R^2 value of 0.95.

$$PEA_2 = \begin{cases} 17.123T + 2.919, & 0.05 \le T < 0.2 \\ -13.292T + 8.895, & 0.2 \le T \le 0.5 \end{cases} \quad (1)$$

For equipment placed on different floors, the acceleration amplification factor is defined as the ratio of the PEA to the Peak Floor Acceleration (PFA) at the corresponding floor. This factor reflects the amplification effect of the equipment structure on the acceleration input from the supporting floor. Fig. 21 presents the acceleration amplification factors for the first- and second-floor equipment. Similar to the average ERS curves, the average amplification factor curves for the first-floor equipment in the X, Y, and bidirectional SRSS directions also exhibit certain fluctuations, without the significant increasing or decreasing trend. The ranges are 2.95–3.96 (X), 3.48–4.19 (Y), and 2.97–3.53 (SRSS), respectively. Among them, the SRSS-combined amplification factor has the narrowest range, indicating that the peak

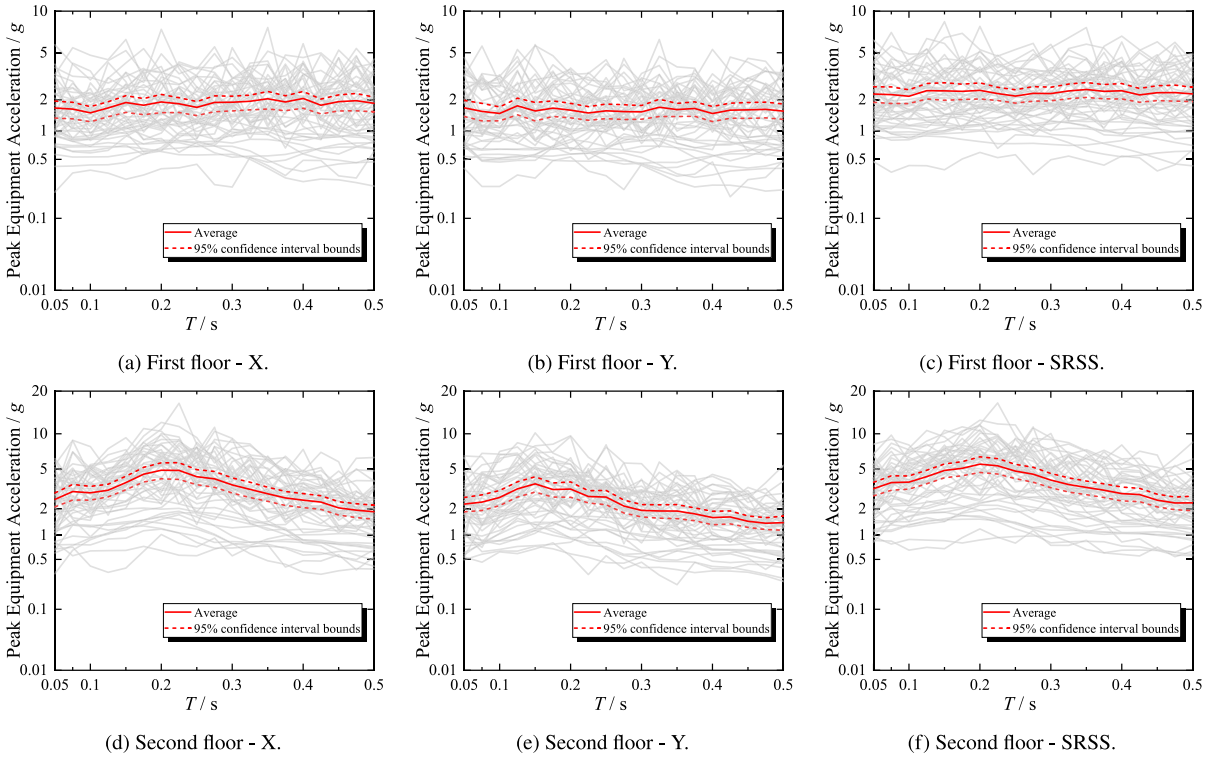

(a) First floor - X. (b) First floor - Y. (c) First floor - SRSS.

(d) Second floor - X. (e) Second floor - Y. (f) Second floor - SRSS.

Fig. 19. Equipment response spectrum.

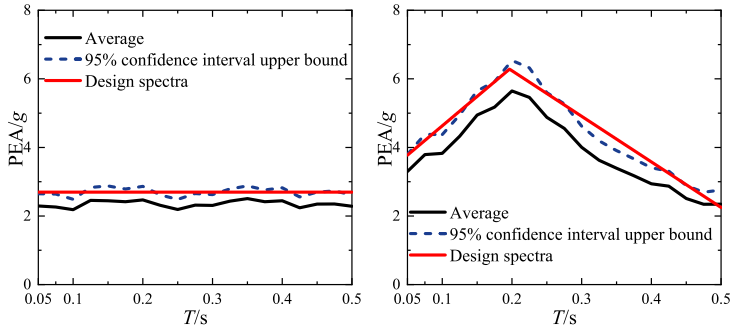

(a) First-floor. (b) Second-floor.

Fig. 20. Recommended design spectrum for equipment.

accelerations in the two horizontal directions do not occur simultaneously. The amplification factor curves for the second-floor equipment exhibit peak-type characteristics, which is consistent with the floor response spectrum characteristics observed for the second floor in the experiment, as shown in Fig. 11. The X-direction curve reaches a maximum of 2.78 at 0.2 s and a minimum of 1.05 at 0.5 s; the Y-direction curve reaches a maximum of 2.75 at 0.15 s and a minimum of 1.11 at 0.5 s; and the SRSS-combined curve peaks at 2.58 at 0.2 s and bottoms at 1.09 at 0.5 s. The maximum of the SRSS-combined curve is the lowest among the three directions, while the minimum values of all curves are relatively close.

Considering that the second-floor equipment is mounted on a support bracket (the blue part beneath the equipment in Fig. 17), unlike the first-floor equipment which is directly installed on the base beam, the potential influence of this bracket on the equipment's response is further investigated. To this end, the stiffness of the support frame is modified by progressively increasing the dimensions of its rectangular steel tube columns from the original 40 × 20 × 3 mm to 60 × 40 × 4 mm and 80 × 60 × 5 mm. The results, as shown in Fig. 22, reveal that the changes in installation stiffness have an insignificant effect on the equipment's acceleration response. Furthermore, the minor influence observed is inconsistent across the different ground motions and varied with the equipment's natural period. This outcome is attributed to the complex dynamic coupling between the ground motion, the primary structure, the support bracket, and the equipment itself. In addition, it can be noted that variations in the support bracket stiffness have little effect on the shape of the acceleration amplification factor curves. Given these findings, it is recommended that for practical engineering applications, the support frame be designed to meet code requirements based on economic principles first, followed by an analysis of the equipment's response to ensure its safety.

Based on the above analysis, since the first-floor equipment exhibits relatively uniform responses across different periods, there is no clearly optimal solution. In contrast, the second-floor equipment typically reaches its maximum response near the fundamental period of the overall structure, and the minimum response often occurs around 0.5 s. Therefore, it is advisable to avoid placing the equipment's natural period near the structural fundamental period and instead select a longer

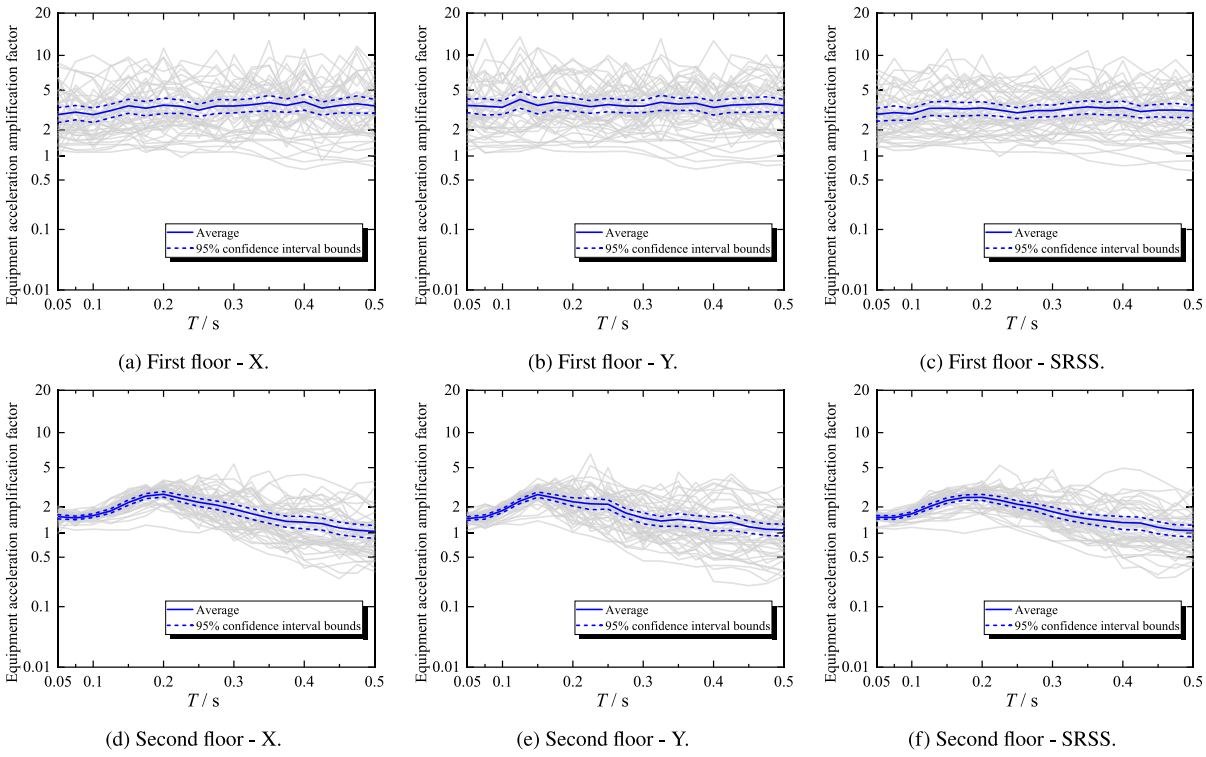

(a) First floor - X. (b) First floor - Y. (c) First floor - SRSS.

(d) Second floor - X. (e) Second floor - Y. (f) Second floor - SRSS.

Fig. 21. Equipment acceleration amplification factor.

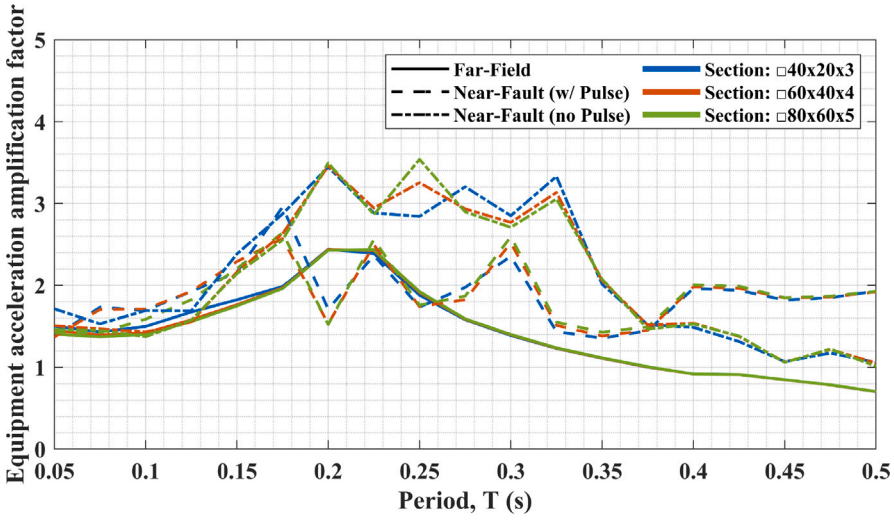

Fig. 22. The influence of different equipment support bracket stiffness on acceleration response.

period where possible. Typically, the natural period of equipment can be adjusted by modifying the stiffness characteristics of the equipment enclosure during the design process.

5. Structural design strategy for prefabricated steel cabin

The topological design of prefabricated cabin structures is typically driven by the functional and maintenance requirements of substations, making them more akin to standardized industrial products rather than conventional buildings. For structural engineers, the key design challenge lies in refining the given structural layout by adjusting beam and column dimensions and incorporating lateral-resisting components to ensure suitability in regions with higher seismic intensity. In light of this, the present study aims to propose a preliminary indicator that characterizes both the structural features of the prefabricated cabin and the properties of ground motion, thereby providing preliminary recommendations for feasible structural design schemes and facilitating the design process of this type of industrial product.

5.1. Response spectrum stiffness ratio η

The seismic response spectrum can reflect both the characteristics of ground motion and the dynamic properties of the structure. Through the acceleration response spectrum, one can roughly estimate the stiffness demands of a structure, while lateral stiffness is a key factor influencing structural displacement response. Therefore, this study proposes a dimensionless parameter, referred to as the “response spectrum stiffness ratio” (η), to define the applicable range of lateral

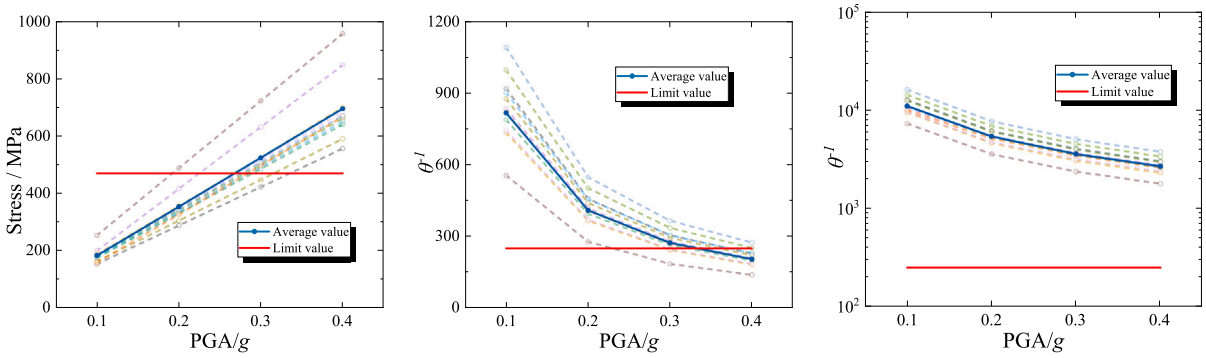

(a) Maximum stress of structural elements. (b) Inter-story drift ratio of the first floor. (c) Inter-story drift ratio of the second floor.

Fig. 23. Calculation results of pure-frame prefabricated cabin structure.

stiffness for the structure. Essentially, η is the ratio between the actual lateral structural stiffness and the stiffness demand derived from the design acceleration response spectrum corresponding to rare-level earthquakes. The calculation formula is as follows:

$$\eta = \frac{K}{(S_a \times M)/(\theta \times H)} \tag{2}$$

where S_a is the rare-level seismic design spectral acceleration corresponding to the fundamental translational period [21]; M is the total mass of the structure; θ is the inter-story drift limit, taken as 1/250; H is the story height; and K is the lateral stiffness of the structure, defined as the ratio of base shear to top-of-structure displacement under an inverted triangular lateral load distribution.

Specifically, according to the State Grid Corporation of China's specification Q/GDW 11882-2018 [29], the cabin door must remain undamaged after an earthquake. Related studies [30] have shown that when the inter-story drift ratio exceeds 1/250, there is approximately a 60% probability that door deformation may hinder evacuation. Considering that the structural prototype studied in this paper is relatively small in scale and the displacement limits used in the experiments are conservative, adopting a drift limit of 1/250 does not necessitate significant reinforcement and still ensures economic feasibility. Additionally, compared to a uniformly distributed load, the inverted triangular distribution better reflects the actual distribution of seismic loads, and is therefore adopted for the calculation of the structure's lateral stiffness.

5.2. Parametric analysis of η

Although the ranges of η calculated under different design seismic intensity levels may overlap, the structural performance and compliance with seismic requirements can still vary. Therefore, the parametric analysis is required for each intensity level. As the experimental results indicate that the tested model was conservatively designed, the analysis first explores the maximum seismic design intensity level that can be satisfied by the prefabricated cabin structure with the lowest lateral stiffness, in order to reduce computational effort. The remaining intensity levels are then analyzed separately. When the structural layout is fixed and cannot be altered, the prefabricated cabin structure with the lowest lateral stiffness corresponds to the configuration without lateral steel plates on either floor, and with both upper and lower modules using hollow square steel columns of 100 × 100 × 4 mm (the minimum section size satisfying the code requirements for width-to-thickness and slenderness ratios [18]). All other structural components remain unchanged. This configuration is hereafter referred to as the "pure-frame prefabricated cabin structure". Finite element simulation results indicate that the first two translational periods of the pure-frame prefabricated cabin structure are 0.270 s and 0.211 s, respectively, compared to 0.202 s and 0.165 s for the tested structure. Therefore, the range of structural variation period considered in subsequent parametric analyses is approximately 0.15 s to 0.3 s.

Ground motion records are selected in accordance with Chinese codes GB 50011-2010 'Code for seismic design of buildings' [21] and GB/T 38591-2020 'Standard for Seismic Resilience Assessment of Buildings' [31], including two artificial ground motions and nine natural ground motions (sourced from FEMA P695 [28]). The basic parameters of the selected ground motions are summarized in Table 5. The selected ground motions (X:Y = 1:0.85) are applied to the pure-frame prefabricated cabin structure.

Fig. 23 illustrates the calculation results of the pure-frame prefabricated cabin structure. In terms of structural stress, as the PGA increases from 0.1 g to 0.4 g, the maximum stress in the structural members shows a linear growth trend. Under all loading cases, the maximum stress consistently occurs at the connection between the lintel ends and the columns. For instance, when PGA reaches 0.3 g, the maximum structural stress is approximately 507 MPa (Fig. 24), which is close to the ultimate strength of Q355 steel (470 MPa). This suggests that reinforcing the lintels or locally strengthening their ends could help mitigate stress concentrations. Meanwhile, the cabin columns remain in the elastic range. Therefore, stress is not considered the critical factor limiting the structural capacity of the prefabricated cabin, and it is concluded that the pure-frame structure can generally satisfy the stress requirements under PGA = 0.3 g. In terms of displacement, the inter-story drift ratios for both the first and second floors increase with the rise in PGA. When PGA reaches 0.4 g, the first-floor drift angle exceeds the allowable limit for the first time, whereas the second-floor drift angle remains relatively small (less than 1/1000) throughout. From an economic perspective, it is thus reasonable to consider omitting the lateral bracing plates on the second floor, and this configuration is adopted in subsequent parametric analyses. In summary, the pure-frame prefabricated cabin structure is deemed capable of withstanding a maximum PGA of 0.3 g, corresponding to seismic design intensity level up to 7 as specified in Chinese code [21].

Subsequently, a parametric analysis of η is conducted under seismic intensity levels of 8 (PGA_{475y} = 0.2 g) and above, aiming to determine the minimum η value required to meet structural demands under rare earthquake scenarios for different seismic intensities. Based on the pure-frame prefabricated cabin structure, the width of the lateral bracing steel plates is adjusted to achieve variations in η. Fig. 25 presents the peak inter-story drift ratio of the first story under seismic intensities of 8 (PGA_{475y} = 0.2 g), 8 (PGA_{475y} = 0.3 g), and 9, corresponding to different η values. The parametric analysis is terminated once the drift angle satisfies the prescribed limit for the first time. As the structural stress is not the governing factor for determining whether the prefabricated cabin structure meets seismic demands, and the inter-story drift angle of the second story remains consistently small, both are not shown here. The results indicate that a minimum η (η_{limit}) of 0.5 is required for a design intensity of 8 (PGA_{475y} = 0.2 g), and a value of 0.45 is required for intensities higher than that.

Table 5
Summary of ground motions information used for parametric analysis of η.

Ground motion	Year	Location	Magnitude	Recording station	PGA/g	PGV/(cm/s)	Duration/s
SAEWS-01	–	–	–	–	0.50	53.1	20.00
SAEWS-02	–	–	–	–	0.50	61.7	20.00
Northridge-01	1994	Northridge	6.7	Canyon country	0.48	45.0	19.99
Kobe	1995	Kobe	6.9	Nishi-Akashi	0.51	37.0	40.96
Kocaeli-01	1994	Kocaeli	7.5	Duzce	0.36	59.0	27.19
San Fernando	1971	San Fernando	6.6	Hollywood Stor.	0.21	19.0	28.00
Irpinia	1980	Irpinia	6.9	Sturno	0.31	45.5	39.34
Kocaeli-02	1999	Kocaeli	7.5	Izmit	0.22	29.8	30.00
Imperial	1979	Imperial	6.5	Bonds corner	0.76	44.3	37.61
Northridge-02	1994	Northridge	6.7	Sepulveda VA	0.73	70.1	47.77
Kocaeli-03	1999	Kocaeli	7.5	Yarimca	0.31	73.0	35.00

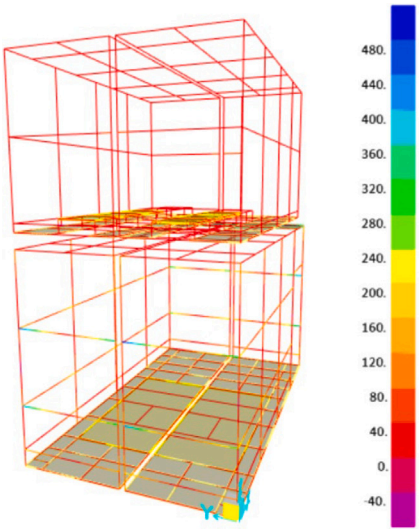

Fig. 24. Structural stress diagram under Kocaeli-03 earthquake (PGA = 0.3 g).

5.3. Design strategy based on η

Based on findings from parametric analyses, the response spectrum stiffness ratio η can be used as a guiding index for the structural design of prefabricated cabins. As illustrated in Fig. 26, the design process can follow two distinct pathways:

1. For seismic design intensity levels of 7 (0.15 g) or below: Previous analysis indicates that the pure-frame prefabricated cabin structure with minimum stiffness is sufficient to meet structural demands. Therefore, member sections can be designed directly based on slenderness and width-to-thickness ratio limits, without the need for additional seismic design.
2. For seismic design intensity levels of 8 (PGA_{475y} = 0.2 g) or above: A preliminary structural design should first be carried out. The η value is then calculated. If $\eta < \eta_{limit}$, the structure should be redesigned — either by increasing member cross-sections or by adding lateral force-resisting components — until $\eta \geq \eta_{limit}$ is achieved.

It should be emphasized that this design method does not replace the structural verification process. Regardless of the seismic intensity level, a full structural check must be conducted after the completion of the design.

6. Summary and conclusions

This paper presents a bidirectional full-scale shaking table test on a prefabricated substation equipment cabin to investigate its key performance characteristics, including structural dynamic properties and the seismic responses of both the cabin structure and the internal equipment. A finite element model of the prefabricated cabin was developed and validated against the experimental data. Based on the validated finite element model and inspired by the concept of floor response spectra, the peak acceleration responses and acceleration amplification factors of equipment with various natural periods inside the cabin were analyzed, leading to a corresponding design strategy for equipment period control. Furthermore, a dimensionless parameter, the response spectrum stiffness ratio (η), was proposed and its threshold values under different seismic intensity levels were determined through parametric analysis, providing an effective strategy for the structural design of prefabricated cabins. The main findings and conclusions can be drawn as follows:

- The tested prefabricated substation equipment cabin is classified as a short-period structure, with natural periods of 0.202 s and 0.165 s in the X and Y directions, respectively. Its damping ratios are relatively higher compared to typical steel structures, measured at 8.7% in the X direction and 6.8% in the Y direction.
- The results of the bidirectional full-scale shaking table test indicate that the prefabricated cabin meets the structural requirements for a seismic intensity of 8 (PGA_{475y} = 0.3 g). The measured structural acceleration amplification factors range approximately from 1.0 to 2.5. Under the rare earthquake scenario, the maximum inter-story drift ratio is 1/319, which satisfies the code-specified limit of 1/50 and provides a considerable safety margin.
- Under the considered scenario with a PGA of 0.51 g, the peak acceleration response and acceleration amplification factor of the switchgear equipment placed on the first floor show some degree of fluctuation across different equipment natural periods, but no clear increasing or decreasing trend is observed overall, making it difficult to reduce the acceleration response by adjusting the equipment's period. In contrast, for the panel-type equipment placed on the second floor, the response curves exhibit a single-peak pattern across different natural periods, suggesting that its acceleration response can be effectively reduced by avoiding the peak period and extending the equipment's natural period.
- Numerical analysis results show that the pure-frame prefabricated cabin module structure, with column sections designed to meet the minimum code requirements for width–thickness and slenderness ratios, can satisfy seismic performance requirements up to a maximum seismic intensity level 7. For structures with an seismic design intensity level 8 (PGA_{475y} = 0.2 g), the minimum required value of the response spectrum stiffness ratio, η, is 0.5; for intensities higher than 8 (PGA_{475y} = 0.2 g), the minimum required η value is 0.45.

In summary, this study provides valuable insights and technical support for the application of prefabricated substation equipment cabins in high seismic intensity regions. However, it also has certain limitations: the investigated prefabricated cabin is relatively small in

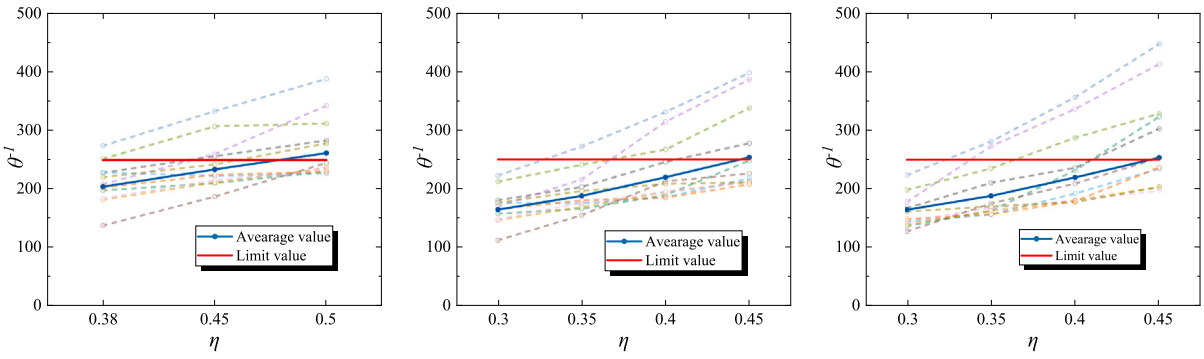

(a) Intensity level 8 (PGA_{475y}=0.2 g). (b) Intensity level 8 (PGA_{475y}=0.3 g). (c) Intensity level 9.

Fig. 25. Peak inter-story drift ratio with different η.

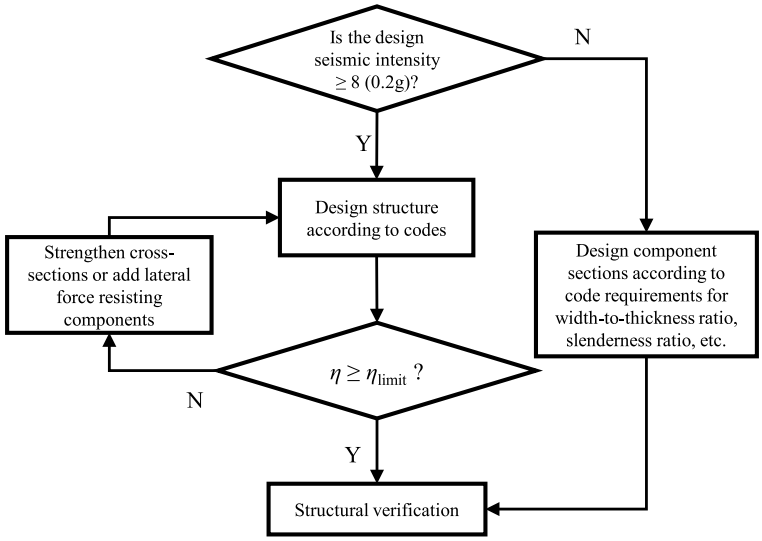

Fig. 26. Design process for prefabricated cabin structures.

size, and the functionality of substation equipment during seismic events was not examined. Future research should focus on exploring the dynamic behavior and fragility analysis of large-scale prefabricated substations composed of multiple modules and integrated with more equipment. This should extend to conducting more detailed, individual seismic performance assessments and fragility constructions for the equipment housed within the prefabricated modules. Furthermore, the effectiveness and potential economic benefits of common mitigation measures, such as seismic isolation, should be investigated for their application to these structures. Ultimately, research should encompass the entire complex and interdependent "structure-equipment" system to deduce its structural and functional losses during an earthquake and to model the post-earthquake recovery process, thereby enabling a holistic evaluation of its seismic resilience.

CRediT authorship contribution statement

Jiajun Du: Writing – original draft, Visualization, Validation, Methodology, Investigation, Data curation. **Wei Wang:** Writing – review & editing, Supervision, Resources, Project administration, Funding acquisition, Conceptualization. **Jiachen Zhang:** Writing – original draft, Visualization, Validation, Software, Methodology, Investigation, Formal analysis, Data curation, Conceptualization. **Xiaotian Liu:** Writing – review & editing, Validation, Software, Methodology, Investigation, Formal analysis, Conceptualization. **Theodoros L. Karavasilis:** Writing – review & editing, Supervision, Resources, Project administration, Funding acquisition, Conceptualization.

Declaration of competing interest

The authors declare that they have no known competing financial interests or personal relationships that could have appeared to influence the work reported in this paper.

Acknowledgments

The financial supports from the National Natural Science Foundation of China (NSFC) with Grant No. 52378182, the Collaborative Research Project under International Joint Research Laboratory of Earthquake Engineering at Tongji University and the Shanghai 2022 Science and Technology Innovation Action Plan Social Development Science and Technology Research Project with Grant No. 22dz1201700 are gratefully acknowledged.

Data availability

Data will be made available on request.

References

[1] Azar R. Substations: Transformations and improvements [In My View]. IEEE Power Energy Mag 2019. http://dx.doi.org/10.1109/MPE.2019.2910423.

[2] Yu Y, Li G, Li P, Zhu Q, Yuan D, Wang C, Li J, Huang H, Li L, Zhang X. Investigation and analysis of electric equipment damage in Sichuan power grid caused by Wenchuan earthquake (in Chinese). Power Syst Technol 2008;(11):5–10.

[3] Zhu W, Bian X, Xie Q. Refined seismic fragility curves of substation equipment considering ground motion classifications. Soil Dyn Earthq Eng 2024;187:108995. http://dx.doi.org/10.1016/j.soildyn.2024.108995.

[4] Taghizadeh M, Delaviz A, Akbarzadeh MR, Estekanchi H. Optimal seismic intensity measure selection for high voltage electrical substation equipment in various setup configurations. Soil Dyn Earthq Eng 2025. http://dx.doi.org/10.1016/j.soildyn.2024.109106.

[5] Li X, Xie Q, Wen J. Double friction pendulum-based isolation optimization for transformer-bushing systems. Eng Struct 2024;320:118909. http://dx.doi.org/10.1016/j.engstruct.2024.118909.

[6] He C, He K, Jiang L, Xie Q, Yang Z. Effects of wire rope isolators on seismic life-cycle cost of UHV bypass switch. Int J Disaster Risk Reduct 2024;114:104917. http://dx.doi.org/10.1016/j.ijdrr.2024.104917.

[7] Liang H, Xie Q. Probabilistic seismic risk analysis of electrical substations considering equipment-to-equipment seismic failure correlations. Reliab Eng Syst Saf 2024;253:110588. http://dx.doi.org/10.1016/j.ress.2024.110588.

[8] Liu X, Xie Q. A multi-strategy framework to evaluate seismic resilience improvement of substations. Reliab Eng Syst Saf 2024;245:110045. http://dx.doi.org/10.1016/j.ress.2024.110045.

[9] Yunnan Qujing Iron and Steel Group Phoenix Co Ltd. 220KV substation. 2025, URL http://www.qjfhgt.com/temp/1583223039692075886.jpg. [Accessed 01 April 2025].

[10] Tgood Co Ltd. Modular smart prefabricated cabin-type substation. 2025, URL http://www.qdtgood.com/office/OA/News/images/Pic/12.jpg. [Accessed 01 April 2025].

[11] ZhangM J, Liu J, Mu H, Jin X, Yang Z, Lin Y. Research on intelligent construction of modular substation. In: 2022 4th international academic exchange conference on science and technology innovation. IAECST, IEEE; 2022, p. 253–6.

[12] Tian X, Wang K, Yao G, Wang H, Zeng T, Mu H, Ju Z, Lu K, Li Y. Exploration of engineering technology advantage and application of prefabricated substations. In: Proceedings of the 2023 4th international conference on big data economy and information management. 2023, p. 651–7.

[13] Li H, Yun F, Li C, yan Gao J, Shishen G, Zhao J. Simulation analysis of strength of double layer structure of prefabricated substation. DEStech Trans Eng Technol Res 2017. http://dx.doi.org/10.12783/DTETR/ICETA2016/7062.

[14] Yang N, Guo S, Niu Y, Wang W. Finite element analysis and optimization design of the base of prefabricated cabin for secondary combination devices, vol. 02, 2017, p. 51–4. http://dx.doi.org/10.1109/IHMSC.2017.127.

[15] Congru Y, Tiange S, Xiaobin S, Xianglin G, Xuwen X. Seismic performance of indoor substation RC frames with combined base isolation techniques. Eng Struct 2023;284:115962. http://dx.doi.org/10.1016/j.engstruct.2023.115962.

[16] Chen S, Guo X, Chae Y, Luo J, Fang Y, Wu Z. Experimental and numerical studies on indoor substation prefabricated steel frames with a partial isolation system. Structures 2025;75:108843. http://dx.doi.org/10.1016/j.istruc.2025.108843.

[17] Feng Y, Zeng Z, Jiang Q, Zeng T, Chong X, Huang J. Shaking table test of prefabricated equipment cabins with a resilient steel frame at the bottom. Eng Struct 2025;322:119019. http://dx.doi.org/10.1016/j.engstruct.2024.119019.

[18] Standardization Administration of the PRC. GB/T 50017-2017 Standard for design of steel structures. China Standards Press; 2017.

[19] Zuo H, Sun G, Zhang P, Wang M, Li J, Shang Q, Wang T. Shaking table tests of a switching power cabinet considering physical damage and functionality loss. Soil Dyn Earthq Eng 2024;177:108421. http://dx.doi.org/10.1016/j.soildyn.2023.108421.

[20] Shang Q, Zuo H, Zhang X, Li Z, Sun G, Zhang P, Li J, Wang T. Shaking table tests of power distribution cabinets: Physical damage, post-earthquake functionality and seismic response evaluation. Structures 2024. http://dx.doi.org/10.1016/j.istruc.2024.106208.

[21] Ministry of Housing and Urban-Rural Development of the PRC. GB/T 50011-2010 Code for seismic design of buildings. China Architecture & Building Press; 2016.

[22] Zhang X, Li Z, Sun G, Zhang P, Zuo H, Shang Q, Wang T. Evaluation of seismic response of server cabinets through shaking table tests. Eng Struct 2024. http://dx.doi.org/10.1016/j.engstruct.2023.117322.

[23] Ministry of Housing and Urban-Rural Development of the PRC. GB/T 50994-2014 standard for aseismatic appraisal of electrical facilities in industrial plants. China Planning Press; 2014.

[24] Wang T, Shang Q, chao Li J. Seismic force demands on acceleration-sensitive nonstructural components: a state-of-the-art review. Earthq Eng Eng Vib 2021;20:39–62. http://dx.doi.org/10.1007/s11803-021-2004-0.

[25] Hao Y, Feng L, Mao C. Study on shaking table tests of a typical telecommunication cabinet (in Chinese). J Seism Res 2020;43:485–90.

[26] Cheng Z, Zhang T, Hu G, Wang K, He Y, Feng Y, Yu F, Zeng Z. Shaking table test and numerical simulation study of secondary equipment cabinet with different connection stiffness (in Chinese). Hebei J Ind Sci Technol 2024;41:450–60.

[27] Iijima T, Abe H, Suzuki K. Seismic fragility capacity of equipment electric panel test. Trans At Energy Soc Jpn 2008;7(2):99–111.

[28] Federal Emergency Management Agency (FEMA). FEMA P695 Recommended Methodology for Quantification of Building System Performance and Response Parameters. Applied Technology Council; 2009.

[29] State Grid Corporation of China. Technical specification for prefabricate cabin pattern 10kV 35kV primary and secondary combination device: Q/GDW 11882-2018. State Grid Corporation of China; 2018.

[30] Xie X, Zhang L, Qu Z. Experimental seismic fragility of windows and doors with plastic-steel frames in masonry infill walls (in Chinese). Earthq Eng Eng Dyn 2019;39:184–91.

[31] Standardization Administration of the PRC. GB/T 38591-2020 standard for seismic resilience assessment of buildings. China Standards Press; 2020.